Ferroelectricity-Induced Coupling between Light and Terahertz-Frequency Acoustic Phonons in $BaTiO_3/SrTiO_3$ Superlattices

A. Bruchhausen,[1] A. Fainstein,[1] A. Soukiassian,[2] D. G. Schlom,[2] X. X. Xi,[2] M. Bernhagen,[3] P. Reiche,[3] and R. Uecker[3]

[1]*Instituto Balseiro & Centro Atómico Bariloche, C.N.E.A., R8402AGP Bariloche, Río Negro, Argentina*

[2]*Materials Research Institute, The Pennsylvania State University, University Park, Pennsylvania, 16802, USA*

[3]*Institute for Crystal Growth, Max-Born-Straße 2, D-12489 Berlin, Germany*

(Received 26 December 2007; published 6 November 2008)

We report a UV-Raman study of folded acoustic vibrations in epitaxial ferroelectric $BaTiO_3/SrTiO_3$ superlattices. The folded acoustic doublets show an anomalous temperature dependence disappearing above the ferroelectric transition, which is tuned by varying the thickness of the $BaTiO_3$ and $SrTiO_3$ layers. A mechanism involving the acoustic phonon modulation of the spatially periodic ferroelectric polarization explains the observed temperature dependence. These results demonstrate the strong coupling between sound, charge, and light in these multifunctional nanoscale ferroelectrics.

DOI: 10.1103/PhysRevLett.101.197402 PACS numbers: 78.20.Hp, 68.65.Cd, 77.84.−s, 78.30.Hv

Reduced size, in combination with electrical and mechanical boundary conditions, can be exploited to tailor the physical properties of nanoscale oxide ferroelectrics [1–6]. Materials that are usually not ferroelectric can become polarized. The critical thickness of ferroelectric thin films can be reduced to a single unit cell in contact with highly polarizable materials [4]. Their transition temperatures T_c can be tuned by hundreds of degrees in superlattices (SLs), their polarization enhanced, and their switching properties modified [1,2,7–9]. $BaTiO_3$ and $SrTiO_3$ oxide multilayers grown with atomically sharp interfaces can be used to produce THz acoustic mirrors and cavities superior to semiconductor SLs [10].

The possibility to engineer the acoustic properties at the nanoscale is particularly attractive in these multifunctional oxides in view of the expected strong coupling of the vibrational, charge, and light degrees of freedom. These materials become strongly piezoelectric below T_c. Additionally, evidence exists of a strong coupling in their bulk form between the acoustic vibrations and the polarization [11,12]. On the other hand, the presence of a *permanent* polarization below T_c leads to a strong linear electro-optic coupling which is proportional to the ferroelectric polarization [13]. These two specific features, namely, a strong coupling between acoustic vibrations and polarization, and between the latter and light, are at the base of an additional and potentially strong elasto-optic coupling operative in the ferroelectric phase [12,14]. This elasto-optic mechanism could be exploited to couple light with high frequency THz phonons in nanostructures where the ferroelectric polarization is modulated in space. We report a detailed investigation of acoustic vibrations in epitaxial $BaTiO_3/SrTiO_3$ SLs using high-resolution ultraviolet (UV) Raman spectroscopy that demonstrates such an intimate relationship between the ferroelectric state and the light generation of THz hypersound in these oxide nanodevices.

Bulk $BaTiO_3$ (BTO) is cubic and paraelectric above $T_c \approx 403$ K, and becomes tetragonal and ferroelectric below T_c. Unstrained bulk $SrTiO_3$ (STO) is paraelectric at all temperatures because of the combined effects of quantum fluctuations and structural transition [15]. The devices studied here are epitaxially grown crystalline SLs as illustrated in the bottom of Fig. 1. The $BaTiO_3/SrTiO_3$ SLs are denoted by (BTO_n/STO_m), where n and m refer to the thickness, in unit cells (u.c.), of the BTO and STO layers, respectively. SLs differ fundamentally from bulk. The strain in the BTO layers induced by STO substrates leads to T_c's larger than bulk. Conversely, T_c is reduced when the number of atomic layers of BTO (n) is decreased as the dipole-dipole interaction between BTO layers becomes weaker. For this same reason thicker STO layers (large m) suppress T_c by reducing the coupling between the polarized BTO layers [16]. By changing the values of n and m, it is possible to tune T_c from 140 to 640 K [8]. The series of samples studied here were conceived to allow for the tuning of T_c essentially by changing n (from $n = 1$ to

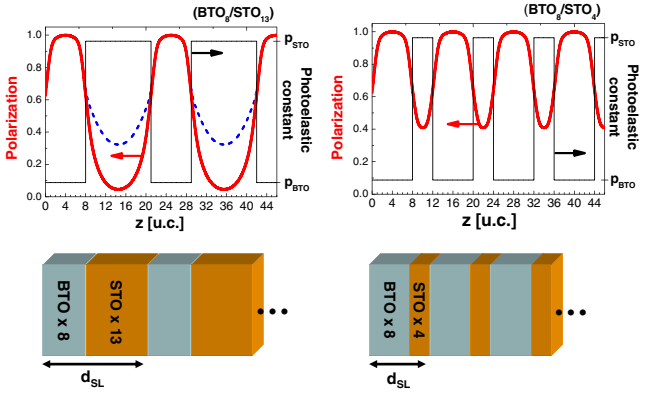

FIG. 1 (color online). Bottom: Schematic of the studied (BTO_n/STO_m) SLs ($n = 1$–8, $m = 4$, 13). Top: Schematic spatial dependence of the photoelastic constants (thin line) and the ferroelectric polarization below T_c (thick curve). The dashed curve indicates the reduction of the polarization modulation for $T \to 0$.

8), while the degree of polarization of the STO layers was varied by controlling m (m being either 4 or 13). The top panel of Fig. 1 illustrates the expected spatial dependence of the ferroelectric polarization in the fully ordered phase [7,16]. The SLs were grown on (001) $SrTiO_3$ substrates (room T lattice parameter $a = 3.905$ Å), except for one which was grown on transparent (110) $GdScO_3$ (room T pseudocubic $a = 3.965$ Å) to allow for forward scattering geometries. Details of the sample preparation by reactive molecular-beam epitaxy and structural characterization have been presented elsewhere [8,10].

To enable the present investigation we have optimized the resolution and throughput of a triple monochromator Raman setup to provide acoustic Raman spectra as close as 10 cm^{-1} to the UV 325 nm line of a HeCd laser, with resolution better than 2 cm^{-1}. Spectra were recorded in subtractive and additive configurations, and both in back and forward scattering geometries from 4–900 K.

A typical Raman spectrum of a BTO_2/STO_{13} SL taken at 5 K is shown in Fig. 2. Visible light excitation only shows spectral features arising from the substrate. In contrast UV excitation at 325 nm (3.81 eV) leads predominantly to signals from the SL due to the added effects of a reduced penetration depth ($\approx$200 nm) and a resonant enhancement ($E_{\mathrm{gap}}^{\mathrm{BTO}} \simeq 3.25$ eV, $E_{\mathrm{gap}}^{\mathrm{STO}} \simeq 3.4$ eV). Strong first-order peaks can be observed below T_c, as exemplified in Fig. 2 with the mode labeled as TO_4. What is noteworthy in this spectrum and is the subject of this Letter is the strong narrow doublet observed at $\sim$40 cm^{-1} and assigned to folded acoustic longitudinal (FA) phonons. Because of the SL periodicity the acoustic phonon branches are folded back into the reduced Brillouin zone enabling their excitation by inelastic light scattering (see the top right panel in Fig. 2) [17]. In addition, gaps are opened at the mini-zone center and border. Wave vector conservation imposes that only phonons with quasimomentum $q = 2k_L$ can be excited in a backscattering (BS) configuration (here k_L is the laser wave vector), while a forward scattering (FS) experiment is required if the zone-center vibrations ($q \approx 0$) are to be probed. The latter requires either transparent or etched substrates [18].

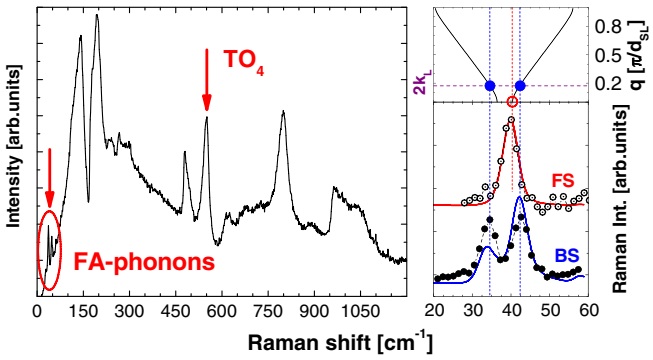

FIG. 2 (color online). Left: UV-Raman spectrum of a BTO_2/STO_{13} SL at 5 K. The FA and TO_4 vibrations are indicated. Right bottom: Back (BS) and forward scattering (FS) FA phonon spectra (293 K) of a BTO_8/STO_4 SL grown on $GdScO_3$. The solid curves are theoretical calculations explained in the text. Right top: FA phonon dispersion [17]. The solid (empty) symbols correspond to the experimentally measured BS (FS) FA phonon peaks.

BS and FS folded acoustic phonon spectra for a BTO_8/STO_4 SL grown on a transparent $GdScO_3$ substrate are shown in the right bottom panel of Fig. 2. The data are compared with theoretical calculations performed with a full photoelastic model that includes the effects of light absorption (complex refractive indices as measured with spectroscopic ellipsometry), electromagnetic, and acoustic boundary conditions [19]. Both the spectral shape and peak positions are nicely reproduced, thus providing the first determination of a THz acoustic mirror performance in ferroelectric oxides. A well-established parity selection rule explains why only one and not two modes are observed at zone center [17]. The observed minigap is almost a factor two larger than typical GaAs/AlAs SLs [10]. We note that we observed, in all the studied samples, only the first zone-center FA doublets. This contrasts with semiconductor SLs where many orders of phonon doublets are observed [17].

The Raman selection rules of optical vibrations in ferroelectrics change at the phase transition. The presence of the first-order TO_4 line in Fig. 2 can be taken as a signature of ferroelectric order, and its disappearance with increasing temperature as a probe of the phase transition [8]. This is illustrated for a (BTO_2/STO_{13}) SL with a transition temperature $T_c \approx 200$ K in Fig. 3. The observation of the optical first-order vibrations below T_c follows from the lifting of inversion symmetry at the phase transition. This symmetry renders the mode Raman forbidden in the paraelectric phase. What is peculiar to these ferroelectric SLs is

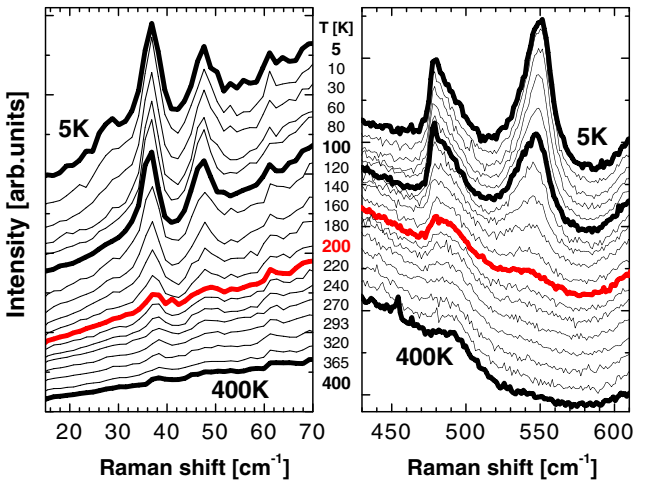

FIG. 3 (color online). Temperature variation of the FA doublet (left) and the TO_4 optical vibration (right) of a BTO_2/STO_{13} SL ($T_c \approx 200$ K). The spectra are vertically shifted for clarity. The corresponding temperatures are given between the panels (spectra for $T = 5$, 100, 200, and 400 K are highlighted to help in their identification).

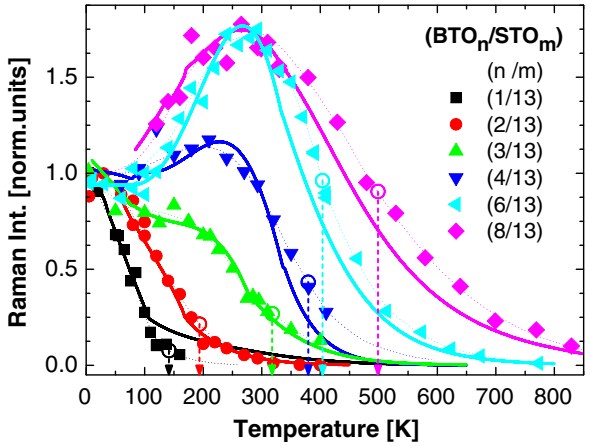

FIG. 4 (color online). Bose corrected temperature dependence of the FA doublet intensity for a series of BTO/STO SLs with $m = 13$, and $n = 1$–8 (normalized to the Raman intensity at $T \rightarrow 0$). The dashed arrows indicate T_c derived from the temperature dependence of the TO_4 peak intensity. The thin dotted curves are guides to the eye. The thick curves correspond to the proposed ferroelectric polarization mediated scattering mechanism (see text for details).

that also the FA doublets *decrease* their intensity with increasing temperature (see Fig. 3). In semiconductor SLs where these FA vibrations have been studied most, it is observed that their intensity *increases* with increasing temperature following the phonon population given by the Bose factor.

We show in Fig. 4 the Bose corrected temperature variation of the FA peak intensity for the SLs studied with $m = 13$ and $n = 1$–8. Each curve is normalized to its respective $T \rightarrow 0$ value. The ferroelectric phase transition temperature T_c, derived from the behavior of the TO_4 peak [8], is shown for the different samples with dashed arrows. It is apparent that, with decreasing temperature, the FA peak intensity follows an onsetlike behavior related to the appearance of the ferroelectric state. Note also that for the three samples with higher T_c the peak intensity does not remain constant once the ferroelectric order is established, but decreases when $T \rightarrow 0$. The acoustic properties of BTO and STO remain essentially unaltered by the relatively small atomic displacements involved in the phase transition. The symmetry of the FA modes, on the other hand, does not change at the phase transition. Thus, a mechanism different from that used to explain the observation of the first-order optical TO_4 mode *only* below T_c (i.e., a symmetry change) must be invoked to explain the observed anomalous temperature behavior of the FA doublets.

The Raman scattering by acoustic phonons is given by [17]

$$\sigma(\omega) \propto [n(\omega) + 1] \left| \int E_S^*(z) \Delta\chi(z) E_L(z) dz \right|^2. \quad (1)$$

$\Delta\chi(z)$ is the change induced in the material dependent dielectric susceptibility by the acoustic phonon strain s, $\Delta\chi(z) = \frac{\partial\chi(z)}{\partial s}\Delta s(z)$ [$s = \frac{\partial u(z)}{\partial z}$, with $u(z)$ the phonon displacement], and $E_L(E_S)$ is the laser (scattered) field. $n(\omega)$ is the statistical Bose-Einstein factor. In semiconductor SLs, the most important mechanism by which the strain modulates χ is the deformation potential interaction: the phonon strain modulates the electronic states, which results in a time dependent variation $\Delta\chi$. The magnitude of this effect is assumed constant in each material, and is expressed by the photoelastic constant $p(z) = \frac{\partial\chi(z)}{\partial s}$ (see the top panels of Fig. 1). The periodicity of $p(z)$ defines the accessible reciprocal lattice vectors and hence the possibility to observe FA vibrations. The intensity of the FA signal, on the other hand, is proportional to the *difference* of $p(z)$ between the two layers in the SL period. As $p(z)$ is only weakly dependent on temperature through the temperature variation of the optical gaps, the main effect of T is given by $n(\omega)$ in Eq. (1). Thus, FA intensities in semiconductor SLs are independent of temperature when the raw experimental data are Bose corrected. In contrast, for the oxide SLs we observe that the measured FA intensities *decrease* and disappear above T_c (see Fig. 4). Since the electronic states determining the dielectric susceptibility are not significantly modified by the ferroelectric transition, the standard photoelastic contribution should not change at T_c. Thus, an additional mechanism is required that has the same periodicity of $p(z)$ (to account for the observation of standard FA doublets), that is absent above T_c, and that is efficient so as to explain the observed strong FA Raman signals.

We propose that the inelastic scattering of FA phonons in these oxide SLs is mediated by the electric polarization P. P^{BTO} develops below T_c in the BTO layers. We assume that P^{BTO} induces a corresponding term in the paraelectric STO layers ($P^{\mathrm{STO}} = \chi_{\mathrm{STO}} P^{\mathrm{BTO}}$) [20]. Thus, as shown in Fig. 1 (top), P displays the same periodicity as the photoelastic constant $p(z)$. In addition to the standard photoelastic mechanism, the dielectric susceptibility in each material can be modulated by the phonon strain through $\Delta\chi(z) = \frac{\partial\chi(z)}{\partial P}\frac{\partial P}{\partial s}\Delta s(z)$. An effective photoelastic constant [14] thus adds to $p(z)$, which is given by $\pi(z) = \frac{\partial\chi(z)}{\partial P}\frac{\partial P}{\partial s}$. Here $\frac{\partial\chi(z)}{\partial P}$ represents the electro-optic constant, which in the ferroelectric phase can be assumed to be linear with P through the quadratic electro-optic effect biased by the polarization [13]. $\frac{\partial P}{\partial s}$ is the piezoelectric coupling which is strong below T_c, but becomes zero above T_c because of the centro-symmetric property of the cubic nonferroelectric phase of the oxides. According to Eq. (1) the Raman intensity by FA phonons should be proportional to the square of the *spatial modulation* of $\pi(z)$. As we show next, all the experimental observations can be consistently accounted for within this model.

Since $\Delta\pi = 0$ above T_c, the FA phonon intensity originated from this mechanism should decay with increasing temperature and disappear above the phase transition, in agreement with the data shown in Fig. 4. The nonobserva-

tion of scattering above T_c implies, in addition, that the deformation potential $p(z)$ is negligible in the studied nanostructures and experimental conditions. As $T \to 0$ the polarization induced in the STO layers increases because of the enhancement of the susceptibility χ_{STO}. This results in a *reduction* in the spatial modulation of P as shown schematically with the dashed curve in the left top panel of Fig. 1. The consequence is a decrease of $\Delta\pi(z)$, and consequently of the Raman intensity as $T \to 0$, as in fact is observed for the SLs studied in Fig. 4. A weak modulation of the polarization at $T = 0$ throughout the SL is consistent with published first-principles density-functional calculations [9]. On the other hand, our results show that the modulation of P increases with temperature, before decreasing as T approaches T_c. This behavior suggests the development of a multidomain state as predicted in Ref. [20]. We have calculated the Raman intensity using Eq. (1), with $\Delta\chi(z)$ given by the proposed P-mediated mechanism. For this purpose we use the fact that $\pi(z) \propto P$ [13,14]. Second, the polarization P^{BTO} is obtained for each sample from the TO_4 phonon intensity which is proportional to P^2 [12,21]. Third, the STO susceptibility χ_{STO} is taken to be the same for all samples and to follow a temperature dependence of the kind given by Ref. [22] (i.e., increasing with decreasing temperature, and saturating when $T \to 0$). And finally, with all these temperature dependencies set, we leave as an adjustable parameter a constant α relating the magnitude of $\pi(z)$ in the BTO and STO layers. The calculated curves are presented with continuous curves in Fig. 4, clearly providing a reasonable description of the data with a minimum of assumptions and free parameters. We note that α for all curves varies only between 0.75 and 1.

The *difference* in ferroelectric polarization between the BTO and STO layers is expected to be smaller for thinner STO spacers (see Fig. 1) [23]. Thus, a smaller m should lead to a weaker spatial modulation $\Delta\pi(z)$ and consequently to a decrease in FA peak intensity. We observe such behavior when comparing the series with $m = 13$ and 4. FA peaks are observable for $n = 1$ and 2 (single and double unit-cell BTO layers) with $m = 13$ but *not* for the thinner $m = 4$ STO spacers. Moreover, for $n = 3$ the FA signals for $m = 4$ are $\approx 40\%$ as intense as those observed in the $m = 13$ sample. These results are also compatible with a stabilizaton of a single-domain state (with a flatter spatial variation of P) for small m [20]. We note in ending that the expected spatial variation of $\pi(z)$ is much more rounded as compared with $p(z)$ (see the top panels in Fig. 1) [23]. This implies that the predominant component of $\Delta\pi(z)$ corresponds to the first reciprocal lattice vector $G = \frac{2\pi}{d_{\mathrm{SL}}}$ (d_{SL} is the SL period), thus providing a possible clue to our observation of *only* the first FA doublets in all the studied oxide SLs.

In conclusion, we have demonstrated that the nanoscale engineering of the ferroelectric polarization in $BaTiO_3/SrTiO_3$ SLs leads to a T-dependent coupling between light and THz folded acoustic vibrations. The observed light scattering mechanism involves the strong piezoelectricity and biased quadratic electro-optic effect existent in these oxides in the ferroelectric state. The inferred T-dependence of the spatial modulation of the polarization for thick $SrTiO_3$ spacer layers is compatible with the development of a multidomain ferroelectric state. Forward scattering experiments reveal the large acoustic mirror stop-bands furthermore establishing the potential of these SL materials for nanophononic devices.

This work was partially supported by the ONR under Grants No. N00014-03-1-0534 (A. F.), No. N00014-03-1-0721, and No. N00014-04-1-0426 (D. G. S.), and by NSF under Grant No. DMR-0507146 (D. G. S. and X. X. X.).

[1] M. Dawber *et al.*, Rev. Mod. Phys. **77**, 1083 (2005).
[2] C. H. Ahn *et al.*, Science **303**, 488 (2004).
[3] J. Junquera and P. Ghosez, Nature (London) **422**, 506 (2003).
[4] D. D. Fong *et al.*, Science **304**, 1650 (2004).
[5] J. H. Haeni *et al.*, Nature (London) **430**, 758 (2004).
[6] K. J. Choi *et al.*, Science **306**, 1005 (2004).
[7] S. Tinte *et al.*, Phys. Rev. B **64**, 235403 (2001).
[8] D. A. Tenne *et al.*, Science **313**, 1614 (2006).
[9] J. B. Neaton and K. M. Rabe, Appl. Phys. Lett. **82**, 1586 (2003).
[10] A. Soukiassian *et al.*, Appl. Phys. Lett. **90**, 042909 (2007).
[11] V. Dvorak, Phys. Rev. **167**, 525 (1968).
[12] P. A. Fleury *et al.*, Phys. Rev. Lett. **26**, 1331 (1971).
[13] M. DiDomenico Jr. and S. H. Wemple, J. Appl. Phys. **40**, 720 (1969).
[14] S. H. Wemple and M. DiDomenico Jr., Phys. Rev. B **1**, 193 (1970).
[15] A. Yamanaka *et al.*, Europhys. Lett. **50**, 688 (2000).
[16] M. Sepliarsky *et al.*, Phys. Rev. Lett. **96**, 137603 (2006).
[17] B. Jusserand and M. Cardona, in *Light Scattering in Solids V*, edited by M. Cardona and G. Güntherodt (Springer-Verlag, Berlin, 1989).
[18] B. Jusserand *et al.*, Phys. Rev. B **33**, 2897 (1986); M. Trigo *et al.*, Phys. Rev. B **66**, 125311 (2002).
[19] J. He *et al.*, Phys. Rev. B **37**, 4086 (1988).
[20] Y. L. Li *et al.*, Appl. Phys. Lett. **91**, 112914 (2007).
[21] K. B. Lyons *et al.*, Phys. Rev. B **17**, 2403 (1978).
[22] K. A. Müller *et al.*, Phys. Rev. B **19**, 3593 (1979).
[23] M. Sepliarsky *et al.*, Phys. Rev. B **64**, 060101 (2001).